PHASE SHIFT DEFECT MODES IN ONE-DIMENSIONAL ASYMMETRICAL PHOTONIC STRUCTURES CONSISTING OF TWO RUGATE SEGMENTS WITH DIFFERENT PERIODICITIES

Y. Y. Liu

College of Physical Science and Technology
Sichuan University, Chengdu, Sichuan 610065, China

Z. Lu

Cornell University
Ithaca, NY 14853, USA

Abstract—A theoretical study of optical properties of phase shift defects in one-dimensional asymmetrical photonic structures consisting of two rugate segments with different periodicities at both normal and oblique incidence is presented. Using the propagation matrix method we numerically calculated transmittance spectra, defect wavelengths, energy density distributions, and group velocities for TE and TM waves, respectively. Our study shows that by adjusting the periodicity of one rugate segment, the defect wavelengths can be shifted toward either a shorter wavelength or a longer wavelength. The differences of the energy density distributions of TE and TM waves at different angles of incidence are explained with the help of group velocity. Effects of the change of the period of one rugate segment on the peak energy densities of defect modes and minimum group velocities at different angles of incidence are also investigated.

1. INTRODUCTION

Photonic crystals that are composed of one-dimensional (1D) periodic dielectric materials of continuously varying refraction index with defect modes have recently received much attention [1–9]. Gradient-index optical materials have been used to fabricate interference filters [1, 2] and environment sensors [10], and potential applications such as

broadband laser protection eyewear and spectral beam splitter have
also been demonstrated [11–13]. Many applications based on 1D
photonic crystals are formed by repeating two or more distinct
homogeneous dielectric layers with different refraction indices [14–33];
however, studies on 1D periodic dielectric structures with smoothly
varying refraction index are still valuable, because of advantages
such as reduced optical losses and better mechanical properties in
contrast to discrete multilayer structures [13, 34–37]. To enlarge the
omnidirectional photonic band gap, porous silicon dielectric mirrors
formed by a periodic repetition of a Gaussian profile refractive index
have been developed [8, 9]. Using the glancing angle deposition
technique (GLAD), narrow bandpass filters have been fabricated with
an introduction of a phase shift defect into a 1D rugate (a sinusoidal
variation of the refraction index) photonic structure [2, 3]. Optical
properties such as defect wavelength and peak transmittance were
investigated both experimentally [2] and theoretically [2, 4, 7] for a 1D
rugate structure of a single period.

In this study, we consider a novel asymmetrical photonic structure
with a phase shift defect located between two distinct rugate segments
with different periodicities. Figure 1 illustrates the profile of refraction
index, and a π phase shift defect is introduced between the rugate
segments A and B. The original period p_A is assigned to the segment
A, and the modified period p_B is to the segment B. The numbers of
cycles of each segment are N_A and N_B, respectively. The refraction
index profile in Figure 1 is described by,

$$n(z) = \begin{cases} n_a + \frac{n_p}{2}\sin\left(\frac{2\pi}{p_A}z + \alpha_0\right), & z \in [0, d_A] \\ n_a + \frac{n_p}{2}\sin\left(\frac{2\pi}{p_B}(z - d_A) + \alpha_0 + \alpha\right), & z \in [d_A, d_B] \end{cases} \quad (1)$$

The average and perturbation indices are denoted by n_a and n_p,
respectively; the original period p_A and the modified period p_B are
related to the design wavelength (λ_0) of the rugate structure via
$p_A = \frac{\lambda_0}{2n_a}$ and $p_B = (1 + \delta)p_A$, where the change of the original period
is denoted by δ; the phase angle at $z = 0$ and the phase shift angle
of the defect are represented by α_0 and α, respectively; the positions
d_A and d_B are $p_A N_A$ and $p_A N_A + p_B N_B$, respectively. The plane of
incidence is assumed to be the x-z plane and the angle of incidence,
θ, is determined by the angle between z direction and the direction
of light incident on the interface at $z = 0$. A monochromatic light is
assumed to be incident from air and outgoing from glass.

The purpose of this theoretical study is to investigate the effects
of the period change of one rugate segment on optical properties of
phase shift defect modes at both normal and oblique incidence. To this

end, using the propagation matrix method [7, 38–42], we numerically calculated transmission spectra, wavelengths at defect modes, energy density distributions, and group velocities for TE and TM waves, respectively, at different angles of incidence. Results from this study are helpful for designing controllable narrow bandpass optical filters and other potential optical applications.

2. METHODS

Closed-form solutions of transmittance (or reflectance) and electromagnetic fields for rugate structures currently are not available in cases of normal and oblique incidence; therefore, we have applied an efficient propagation matrix method to studying optical properties of phase shift defect modes in the proposed rugate photonic structures in Figure 1. Formulations of numerically evaluating transmittance and energy density distributions for TE and TM waves in continuously gradient-index optical materials using the efficient propagation matrix method have been given in the previous studies [7, 42], so, we skip this part here and readers interested in details are referred to therein.
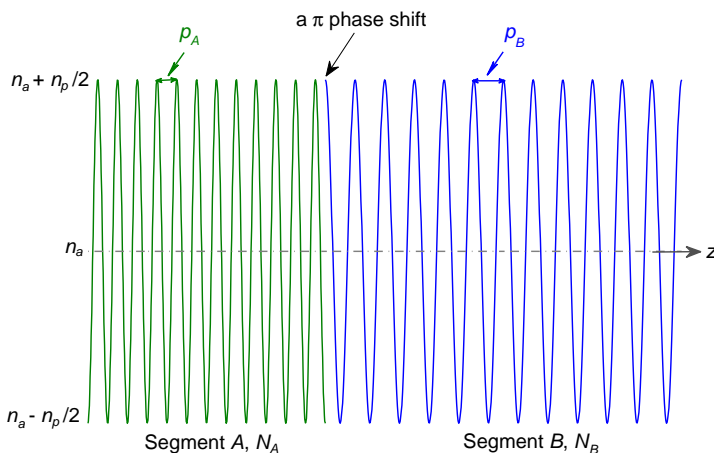

Figure 1. A schematic of the refraction index profile in an asymmetrical photonic structure consisting of two distinct rugate segments with two different periodicities ($\alpha_0 = -\pi/2$ and $\alpha = \pi$).

The group velocity, V_g, against the wavelength of the incident light is calculated using the transmission coefficient, $t = x + iy = T^{1/2}\exp(i\phi)$, where the transmittance T is the module of the transmission coefficient, i.e., $T = |t| = (x^2 + y^2)^{1/2}$. The phase factor of

the transmission coefficient ($\phi = \arctan(y/x)$) is related to the effective wave number k via $\phi = kd_{tot} + \phi_0$, where ϕ_0 represents the shifted phase and the total thickness of the asymmetric rugate structure is $d_{tot} = d_B$. Using the definition of group velocity and $\omega = \frac{2\pi c}{\lambda}$ we find [43, 44],

$$V_g = \frac{d\omega}{dk} = -\frac{2\pi c}{\lambda^2} d_{tot} \frac{x^2 + y^2}{\frac{dy}{d\lambda}x - \frac{dx}{d\lambda}y}. \tag{2}$$

In numerical calculations, a central difference formula is used to replace the differential derivatives in Equation (2), $\frac{df}{d\lambda}|_{\lambda=a} = \frac{f(a+h)-f(a-h)}{2h}$.

3. RESULTS AND DISCUSSION

Parameter values of the asymmetrical rugate structures in Figure 1 are defined in Table 1. In the present study, we consider a small change of the period of the rugate segment B as our numerical example: the change can be either positive (increasing period, $\delta = 1/22$) or negative (decreasing period, $\delta = -1/22$), and other values of the period change (δ) are still possible. We then compare the optical properties of defect modes for these two rugate structures to that of the rugate structure without period change ($\delta = 0$). In addition, we consider only a π phase shift defect because it has been shown that the strongest resonant mode occurs at the π phase shift defect [2, 4, 7].

Table 1. Values and definitions of parameter used in the study.

Symbol	Value	Definition
λ_0	550 nm	Design wavelength of the rugate segment A
n_a	2.0	Average refraction index
n_p	0.52	Perturbation index
n_i	1.0	The incident medium (air)
n_t	1.53	The outgoing medium (glass)
p_A	137.5 nm	The period of the rugate segment A
δ	$\frac{1}{22}, 0, -\frac{1}{22}$	The period change of the rugate segment B
N_A	12	The number of cycles in the rugate segment A
N_B	12	The number of cycles in the rugate segment B
α	π	Phase shift angle
θ	$0 - 90°$	The angle of incidence

3.1. Wavelengths and Transmittance of Defect Modes

3.1.1. TE Wave

Transmittance spectra of three different rugate structures with a π phase shift defect for TE wave at six different angles of incidence from $0°$ to $75°$ with step size of $15°$ are shown in Figure 2(a). In each panel of Figure 2(a), there are three transmission spectra which correspond to three different period changes of the rugate segment B, $\delta = -\frac{1}{22}$ ($p_B = p_A - 6.25$ nm, blue dash-dotted), $\delta = 0$ ($p_B = p_A$, green solid)), and $\delta = -\frac{1}{22}$ ($p_B = p_A + 6.25$ nm, red dashed). In case of normal incidence, when there is no period change (green solid), the resonant wavelength within the stop band is 553 nm. When the period of the rugate segment B slightly decreases, $p_B = p_A - 6.25$ nm, the resonant wavelength shifts to a shorter wavelength (blue dash-dotted), 540 nm; when the period slightly increases, $p_B = p_A + 6.25$ nm, the resonant wavelength moves to a longer wavelength (red dashed), 565 nm. In case of oblique incidence, similar shifting behaviors of resonant wavelengths within the stop band are also found. In addition, the full bandwidth of the stop band increases for the three different rugate structures with the increment of the angle of incidence.

Figure 2(b) shows how resonant wavelength and peak transmittance are changed when the angle of incidence varies. It is clearly shown that resonant wavelengths for each rugate structure ($\delta = -\frac{1}{22}$, 0, or $\frac{1}{22}$) have a blue shift when the angle of incidence increases. Peak transmittance of defect modes is close to 1 and decreases slowly unless a large angle of incidence is reached.

The shifting behaviors of resonant wavelengths of defect modes dependent on the period change of the rugate segment B at any angle of incidence can be physically understood as follows. The periods of rugate segments A and B are related to the design wavelength λ_0 via,

$$p_A = \frac{\lambda_0}{2n_a}, \quad p_B = \frac{(1+\delta)\lambda_0}{2n_a} = \frac{\lambda_0'}{2n_a}, \tag{3}$$

where the λ_0' is the modified design wavelength of the rugate segment B. If the period of rugate segment B changes, the λ_0' varies as well. In our study, when the p_B decreases slightly, i.e., $p_B - p_A = -6.25$ nm, the λ_0' reduces down to 525 nm; while the p_B increases slightly, i.e., $p_B - p_A = +6.25$ nm, the λ_0' increases up to 575 nm. In case of normal incidence, when the period of rugate segment B decreases ($p_B < p_A$), the stop band of the rugate segment B moves to a range of shorter wavelengths, consequently, the resonant wavelength moves to a shorter wavelength (from 553 to 540 nm). When the period of the rugate segment B increases ($p_B > p_A$), the stop band of the rugate segment
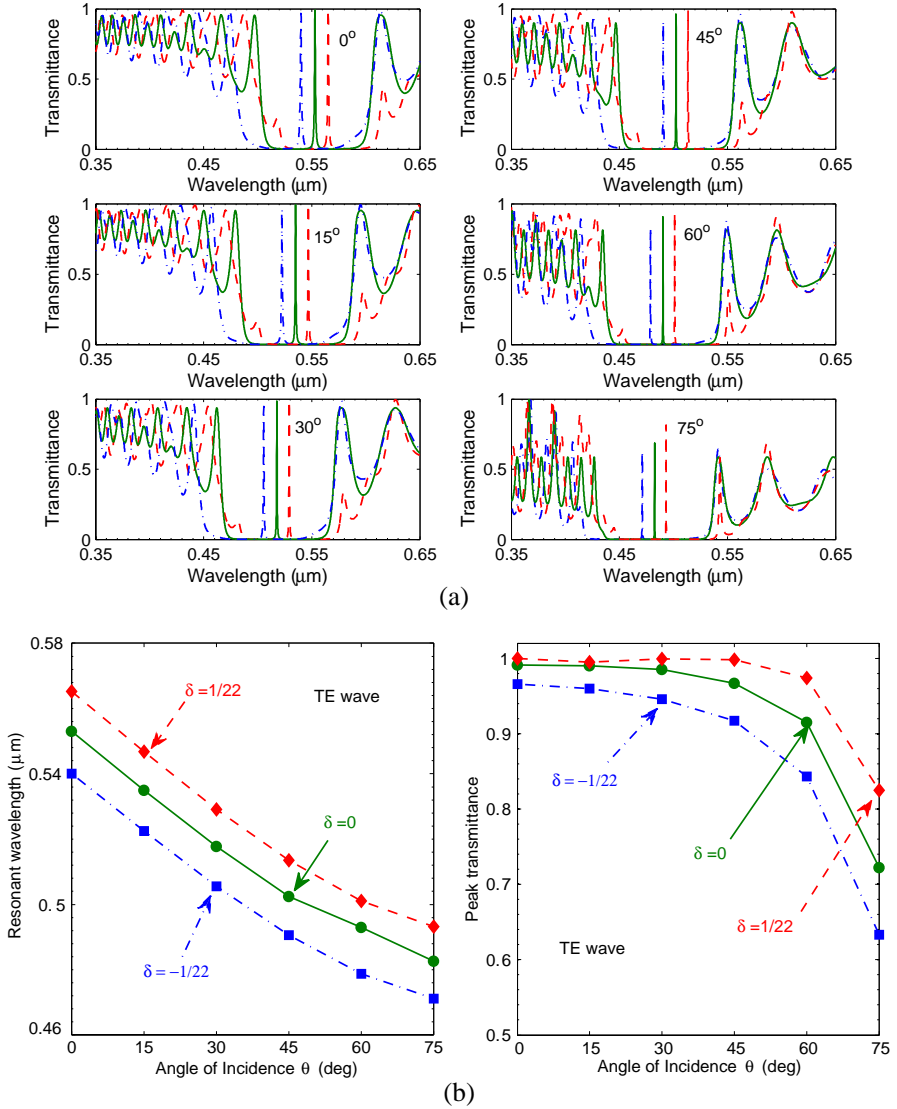
Figure 2. (a) Transmittance of TE wave at six different angles of incidence, 0°, 15°, 30°, 45°, 60°, and 75°. The period changes of the rugate segment B are: $\delta = -\frac{1}{22}$ (blue dash-dotted), 0 (green solid), and $\frac{1}{22}$ (red dashed). (b) Resonant wavelength and peak transmittance against the angle of incidence.

B moves to a range of longer wavelengths, therefore, the resonant wavelength moves to a longer wavelength (from 553 to 565 nm). In case of oblique incidence, this shifting behavior (either blue or red shifts) of defect modes can also be explained similarly. The period change of the rugate segment B, δ, may take different values rather than $\delta = \pm 1/22$ used in this study. The more positive the δ is ($\delta > 1/22$), the more red shift the resonant wavelength has; the more negative the δ is ($\delta < -1/22$), the more blue shift the resonant wavelength gets. However, the range of δ should be limited within the stop band of the rugate structure with no period change ($\delta = 0$).

The blue shift behavior of resonant wavelengths for each of three rugate structures shown in Figure 2(b) may be understood by an approximate analytical expression (with the condition of $n_p \ll n_a$) [45],

$$\lambda_\theta = \lambda_0 \left(1 - \frac{\sin^2 \theta}{n_a^2} \right)^{1/2}. \tag{4}$$

Equation (4) illustrates that at oblique incidence the design wavelength, λ_θ, is a monotonically decreasing function of the angle of incidence, θ. Since the resonant wavelength is very close to the design wavelength, it is expected that a blue shift of the resonant wavelength occurs when the angle of incidence increases. The angular-dependent peak transmittance of defect modes for TE wave can be interpreted as: when the angle of incidence increases, large reflectance is expected and the peak transmittance therefore decreases.

For the observed angle-dependence of the bandwidth for TE wave for three rugate structures, we may understand it using the following approximate analytical expression (with the condition of $n_p \ll n_a$) [45],

$$\Delta \lambda = \lambda_0 \frac{n_p}{2n_a} \frac{1}{\left(1 - \frac{\sin^2 \theta}{n_a^2} \right)^{1/2}}. \tag{5}$$

From this expression, we know that the full bandwidth for TE wave, $\Delta \lambda$, is a monotonically increasing function of the angle of incidence, θ. Thus, when the θ increases, the bandwidth is enlarged.

3.1.2. TM Wave

Transmittance spectra of three different rugate structures with a π phase shift defect in Figure 1 for TM wave at six different angles of incidence from $0°$ to $75°$ with step size of $15°$ are shown in Figure 3(a). In each panel of Figure 3(a), a similar notation for three transmission spectra is used as in Figure 2(a): red dashed ($\delta = \frac{1}{22}$), green solid ($\delta = 0$), and blue dash-dotted ($\delta = -\frac{1}{22}$). In both normal and oblique
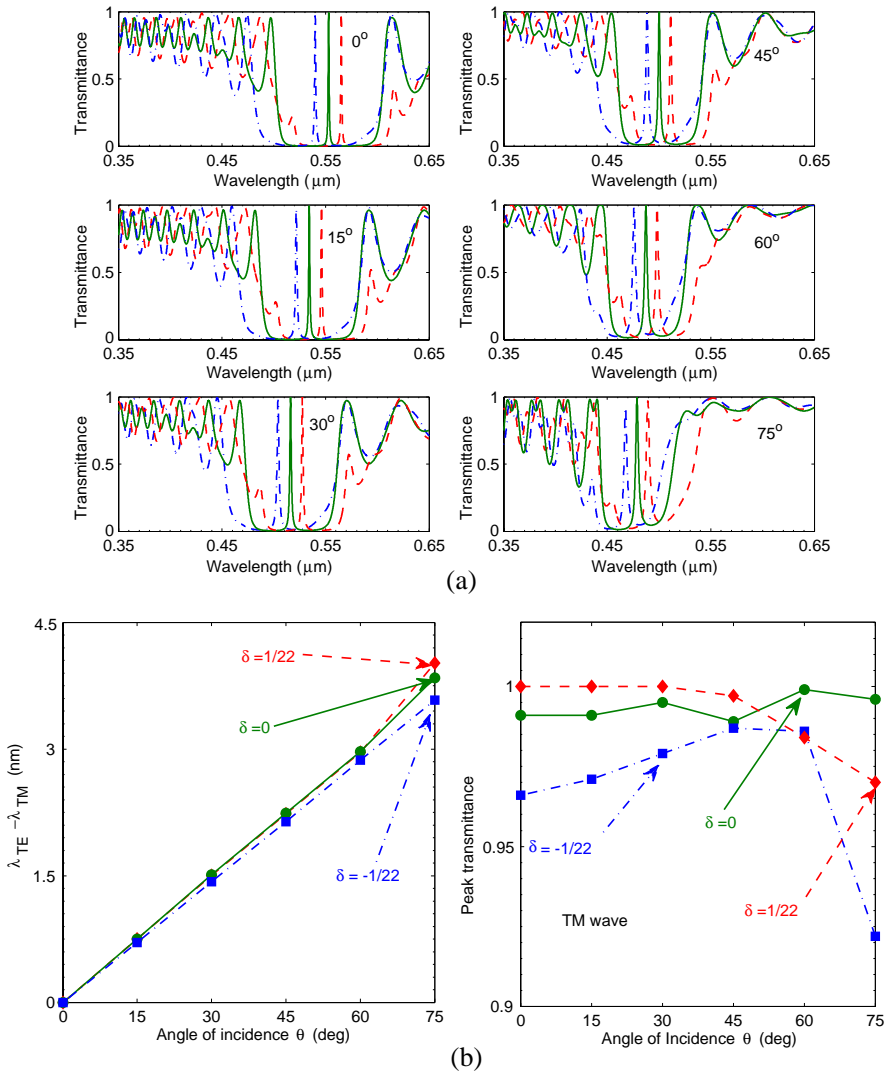
Figure 3. (a) Transmittance of TM wave at six different angles of incidence, $0°$, $15°$, $30°$, $45°$, $60°$, and $75°$. The period changes of the rugate segment B are: $\delta = -\frac{1}{22}$ (blue dash-dotted), 0 (green solid), and $\frac{1}{22}$ (red dashed). (b) Differences of the resonant wavelengths for TE and TM waves and peak transmittance against the angle of incidence.

incidence for TM wave, a similar result of the shifting behavior of resonant wavelength due to the period change at any angle of incidence is found as in the case of TE wave: when reducing the period of the rugate segment B ($\delta = -\frac{1}{22}$), the resonant wavelength has a blue shift, and when increasing the period of the rugate segment B ($\delta = \frac{1}{22}$), the resonant wavelength has a red shift. However, the bandwidth for TM wave becomes narrower with the increment of the angle of incidence, which is different from TE wave.

For each of three rugate structures, an almost identical blue shift of resonant wavelengths for TM wave at different angles of incidence is observed (not given) as found in the case of TE wave. In the left panel of Figure 3, the subtle differences of the resonant wavelengths for TE and TM waves are plotted. The difference of resonant wavelengths linearly increases with the increment of the angle of incidence, from 0 to a few nanometers. It is found that the period change of the rugate segment B has no effect on the difference of resonant wavelengths for TE and TM waves ($\lambda_{\text{TE}} - \lambda_{\text{TM}}$) until a large angle of incidence (75°) reaches. The peak transmittance of defect modes for TM wave (the right panel of Figure 3(b)) is nearly to 1 at all six different angles of incidence. Compared to the case of TE wave, even at a large angle of incidence, the peak transmittance is still high, however, the ability to be a narrow bandpass optical filter reduces, because the full width at half maximum of defect modes becomes broader.

The blue or red shifts of resonant wavelength due to different period changes of the rugate segment B for TM wave can be understood similarly as in the case of TE wave. The blue shift of resonant wavelength for each of three rugate structures may also be explained as for TE wave. The almost complete peak transmittance (close to 1, in the right panel of Figure 3(b)) for TM wave at each different angle of incidence is ascribed to the impedance match — reflectance is close to zero due to the whole rugate structure is nearly matched to the incident medium (air) [30].

The angle-dependence of the full bandwidth for TM wave may be physically understood using the following approximate analytical expression (with the condition of $n_p \ll n_a$) [45],

$$\Delta\lambda = \lambda_0 \frac{n_p}{2n_a} \frac{1 - \frac{2\sin^2\theta}{n_a^2}}{\left(1 - \frac{\sin^2\theta}{n_a^2}\right)^{1/2}}. \tag{6}$$

This expression shows that the bandwidth for TM wave, $\Delta\lambda$, is a monotonically decreasing function of the angle of incidence, θ, therefore, when the θ increases, the bandwidth for TM wave becomes narrower.
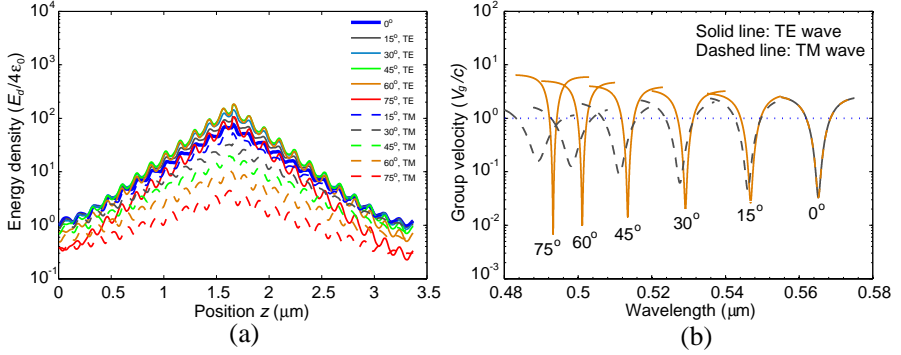
Figure 4. (a) Energy density distributions within the asymmetrical rugate structure in Figure 1 at defect modes for TE and TM waves at six different angles of incidence. (b) Group velocities against the wavelength for TE (solid) and TM (dashed) at six different angles of incidence. The period of the rugate segment B is $p_B = (1 + 1/22)p_A$.

3.2. Energy Density Distribution and Group Velocity

Figure 4(a) shows the energy density distributions at defect modes for TE and TM waves at six different angles of incidence when the period of the rugate segment B is $p_B = (1 + 1/22)p_A$. In general, the energy density peaks at the defect physical location, and exponentially decreases to both ends of the rugate structure shown in Figure 1. For TE wave, the peak energy density becomes higher as the angle of incidence increases, but for TM wave, the energy density declines. Group velocities for TE and TM waves at six different angles of incidence are illustrated in Figure 4(b). When the angle of incidence increases, the minimal group velocity at the resonant wavelength decreases for TE wave, while it increases for TM wave. The contrary patterns of group velocity and energy density may be understood as follows. In this study we consider the proposed photonic structure is lossless, therefore, the energy flux is conserved at the resonant wavelength and the group velocity is inversely related to the energy density [14, 15, 46, 47]. Group velocity also provides information of time delay of the light transmission at resonant modes; the smaller the group velocity is, the longer time the response may take [44].

To further examine the impact of the period change of the rugate segment B on the peak (maximum) energy density and minimum group velocity, we consider two period changes ($\delta = \pm 1/22$) and a non-period change ($\delta = 0$, $p_B = p_A$) in Figure 5. The upper panel of Figure 5 shows that when the period of rugate segment B

slightly increases, $p_B = (1 + 1/22)p_A$, the peak energy density for TE wave increases as well. When the period rugate segment B slightly decreases, $p_B = (1 - 1/22)p_A$, the peak energy density for TE wave reduces, and it is nearly 50% lower than that of the period change with $p_B = (1 + 1/22)p_A$. The peak energy densities for TM waves at different angles of incidence almost overlap for the rugate structures with $p_B = (1 + 1/22)p_A$ and $p_B = p_A$, but a relatively large difference between $p_B = (1 - 1/22)p_A$ and $p_B = p_A$ is found when the angle of incidence is close to zero. The pattern of peak energy density influenced by the period change of the rugate segment B shown in the upper panel of Figure 5 is confirmed by the pattern of minimum group velocity illustrated in the lower panel of Figure 5 (notice a log scale used for group velocity).
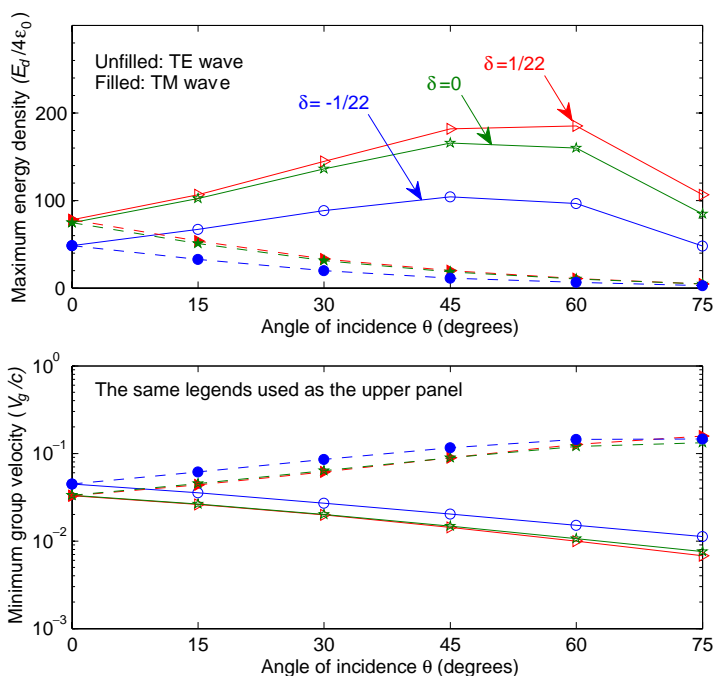

Figure 5. Effects of the period change on the maximum energy densities (upper panel) and the minimum group velocities (lower panel) for TE (unfilled circle, star and triangle) and TM (filled circle, star and triangle) at six different angles of incidence. The period changes of the rugate segment B are: $\delta = -\frac{1}{22}$ (blue circle), 0 (green star), and $\frac{1}{22}$ (red triangle).

The effect of the numbers of cycles of rugate segments A and B on the peak transmittance, peak energy density, and group velocity is not investigated in this study, however, we want to point out that appropriately increasing number of cycles usually results in a better quality of defect modes, stronger peak energy density and slower group velocity.

4. CONCLUSION

We have presented a theoretical analysis of optical properties of a phase shift defect mode in a 1D asymmetrical photonic structure consisting of two rugate segments with different periodicities at both normal and oblique incidence using the propagation matrix method. This study shows that by adjusting the periodicity of one rugate segment, the defect wavelengths can be shifted toward either a shorter wavelength or a longer wavelength, depending on the period change. The differences of the energy density distributions of TE and TM waves at different angles of incidence are explained using the concept of group velocity.

REFERENCES

1. Van Popta, A. C., M. M. Hawkeye, J. C. Sit, and M. J. Brett, "Gradient-index narrow-bandpass filter fabricated with glancin-gangle deposition," *Opt. Lett.*, Vol. 29, 2545–2547, 2004.

2. Hawkeye, M. M. and M. J. Brett, "Narrow bandpass optical optical filters fabricated with one-dimensionally periodic inhomogeneous thin films," *J. Appl. Phys.*, Vol. 100, 044322, 2006.

3. Hawkeye, M. M. and M. J. Brett, "Glancing angle deposition: Fabrication properites, and applications of micro- and nanostructured thin films," *J. Vac. Sci. Technol. A*, Vol. 25, 1317–1335, 2007.

4. Tabunshchyk, K. V., M. M. Hawkeye, A. Kovalenko, and M. J. Brett, "Three-dimensional simulation of periodically structured thin films with uniaxial symmetry," *J. Phys. D: Appl. Phys.*, Vol. 40, 4936–4942, 2007.

5. Brett, M. J. and M. M. Hawkeye, "Materials science. New materials at a glance," *Science*, Vol. 319, 1192–1193, 2008.

6. Hawkeye, M. J., R. Joseph, J. C. Sit, and M. J. Brett, "Coupled defects in one-dimensional photonic crystal films fabricated with glancing angle deposition," *Opt. Express*, Vol. 18, 13220–13226, 2010.

7. Liu, Y. and Z. Lu, "Properties of phase shift defects in one-dimensional rugate photonic structures," *Progress In Electromagnetics Research*, Vol. 111, 213–228, 2011.

8. Estevez, J. O., J. Arriaga, A. Mendez Blas, and V. Agarwal, "Omnidirectional photonic bandgaps in porous silicon based mirrors with a Gaussian profile refractive index," *Appl. Phys. Lett.*, Vol. 93, 191915, 2008.

9. Estevez, J. O., J. Arriaga, A. Mendez Blas, and V. Agarwal, "Enlargement of omnidirectional photonic bandgap in porous silicon dielectric mirrors with a Gaussian profile refractive index," *Appl. Phys. Lett.*, Vol. 94, 061914, 2009.

10. De Stefano, L., L. Moretti, A. Lamberti, O. Longo, M. Rocchia, A. M. Rossi, P. Arcari, and I. Rendina, "Optical sensors for vapors, liquids, and biological molecules based on porous silicon technology," *IEEE Trans. Nanotechnol.*, Vol. 543, 49–54, 2004.

11. Imenes, A. G. and D. Mills, "Spectral beam splitting technology for increased conversion efficiency in solar concentrating systems: A review," *Sol. Energy Mater. Sol. Cells*, Vol. 84, 19–69, 2004.

12. Imenes, A. G., D. Buie, and D. R. Mckenzie, "The design of broadband, wide-angle interference filters for solar concentrating systems," *Sol. Energy Mater. Sol. Cells*, Vol. 90, 1579–1606, 2006.

13. Imenes, A. G. and D. R. McKenzie, "Flat-topped broadband rugate filters," *Applied Optics*, Vol. 45, 7841–7850, 2006.

14. Joannopoulos, J. D., S. G. Johnson, J. N. Winn, and R. D. Meade, *Photonic Crystals: Modling the Flow of Light*, 2nd edition, Princeton University Press, 2008.

15. Yariv, A. and P. Yeh, *Photonics*, Oxford University Press, New York, 2007.

16. Deopura, M., C. K. Ullal, T. Temelkuran, and Y. Fink, "Dielectric omnidirectional visible reflector," *Opt. Lett.*, Vol. 26, 1197–1199, 2001.

17. Fink, Y., J. N. Winn, S. Fan, C. Chen, J. Michel, J. D. Joannopoulos, and E. L. Thomas, "A dielectric omnidirectional reflector," *Science*, Vol. 282, 1679–1682, 1998.

18. Winn, J. N., Y. Fink, S. Fan, and J. D. Joannopoulos, "Omnidirectional reflection from a one-dimensional photonic crystal," *Opt. Lett.*, Vol. 23, 1573–1575, 1998.

19. Srivastava, R., S. Pati, and S. P. Ojha, "Enhancement of omnidirectional reflection in photonic crystals heterostructures," *Progress In Electromagnetics Research B*, Vol. 1, 197–208, 2008.

20. Srivastava, R., K. B. Thapa, S. Pati, and S. P. Ojha, "Omni-

direction reflection in one dimensional photonic crystal," *Progress In Electromagnetics Research B*, Vol. 7, 133–143, 2008.

21. Awasthi, S. K., U. Malaviya, S. P. Ojha, N. K. Mishra, and B. Singh, "Design of a tunable polarizer using a one-dimensional nano sized photonic bandgap structure," *Progress In Electromagnetics Research B*, Vol. 5, 133–152, 2008.

22. Srivastava, R., K. B. Thapa, S. Pati, and S. P. Ojha, "Design of photonic band gap filter," *Progress In Electromagnetics Research*, Vol. 81, 225–235, 2008.

23. Awasthi, S. K., U. Malaviya, S. P. Ojha, N. K. Mishra, and B. Singh, "Design of a tunable polarizer using a one-dimensional nano sized photonic bandgap structure," *Progress In Electromagnetics Research B*, Vol. 5, 133–152, 2008.

24. Banerjee, A., "Enhanced temperature sensing by using one-dimensional ternary photonic band gap structures," *Progress In Electromagnetics Research Letters*, Vol. 11, 129–137, 2009.

25. Wu, C.-J., B.-H. Chu, and M.-H. Weng, "Analysis of optical reflection in a chirped distributed Bragg reflector," *Journal of Electromagnetic Waves and Applications*, Vol. 23, No. 1, 129–138, 2009.

26. Wu, C.-J., B.-H. Chu, M.-T. Weng, and H.-L. Lee, "Enhancement of bandwidth in a chirped quarter-wave dielectric mirror," *Journal of Electromagnetic Waves and Applications*, Vol. 23, No. 4, 437–447, 2009.

27. Wu, C.-J., J.-J. Liao, and T.-W. Chang, "Tunable multilayer Fabry-Perot resonator using electro-optical defect layer," *Journal of Electromagnetic Waves and Applications*, Vol. 24, No. 4, 531–542, 2010.

28. Wu, C.-J. and Z.-H. Wang, "Properties of defect modes in one-dimensional photonic crystals," *Progress In Electromagnetics Research*, Vol. 103, 169–184, 2010.

29. Wu, C.-J., Y.-N. Rau, and W.-H. Han, "Enhancement of photonic band gap in a disordered quarter-wave dielectric photonic crystal," *Progress In Electromagnetics Research*, Vol. 100, 27–36, 2010.

30. Hsu, H. T., T. W. Chang, T. J. Yang, B. H. Chu, and C. J. Wu, "Analysis of wave properties in photonic crystal narrowband filters with left-handed defect," *Journal of Electromagnetic Waves and Applications*, Vol. 24, No. 16, 2285–2298, 2010.

31. Dai, G. L. and M. Y. Xia, "An investigation of quarter-wavelength square-spiral resonator and its applications to miniaturized bandpass filters," *Journal of Electromagnetic Waves*

and Applications, Vol. 24, No. 10, 1303–1313, 2010.

32. Archuleta-Garcia, R., D. Moctezuma-Enriquez, and J. Manzanares-Martinez, "Enlargement of photonic band gap in porous silicon dielectric mirrors," *Journal of Electromagnetic Waves and Applications*, Vol. 24, Nos. 2–3, 351–361, 2010.

33. Manzanares-Martinez, J., R. Archuleta-Garcia, P. Castro-Garay, D. Moctezuma-Enriquez, and E. Urrutia-Banuelos, "One-dimensional photonic heterostructure with broadband omnidirectional reflection," *Progress In Electromagnetics Research*, Vol. 111, 105–117, 2011.

34. Southwell, W., "Using apodization functions to reduce sidelobes in rugate filters," *Applied Optics*, Vol. 28, 5091–5094, 1989.

35. Abu-Safia, H., A. Al-Sharif, and I. Abu-Aljarayesh, "Rugate filter sidelobe suppression using half-apodization," *Applied Optics*, Vol. 32, 4831–4835, 1993.

36. Kennedy, S. and M. M. Brett, "Porous broadband antireflection coating by glancing angle deposition," *Applied Optics*, Vol. 42, 4573–4579, 2003.

37. Vernhes, R., O. Zabeida, J. Klemberg-Spaieha, and L. Martinu, "Single-material inhomogeneous optical filters based on microstructural gradients in plasma-deposited silicon nitride," *Applied Optics*, Vol. 43, 97–103, 2004.

38. Berreman, D. W., "Optics in stratified and anisotropic media: 4×4 matrix formulations," *J. Opt. Soc. Am.*, Vol. 62, 502–510, 1972.

39. Abdulhalim, I., "Analytical propagtion matrix method for linear optics of arbitrary biaxial layered media," *J. Opt. A: Pure Appl. Opt.*, Vol. 1, 646–653, 1999.

40. Lu, Z., "Accurate and efficient calculation of light propagation in one-dimensional inhomogeneous anisotropic media through extrapolation," *J. Opt. Soc. Am. A*, Vol. 24, 236–242, 2007.

41. Lu, Z., "Accurate calculation of reflectance spectra for thick onedimensional inhomogeneous optical structures and media: Stable propagation matrix method," *Opt. Lett.*, Vol. 33, 1948–1950, 2008.

42. Lu, Z., "Efficient 4×4 propagation matrix method using a fourth-order symplectic integrator for the optics of one-dimensional continuous inhomogeneous materials," *Progress In Electromagnetics Research Letters*, Vol. 14, 1–9, 2010.

43. Bendickson, J. M. and J. P. Dowling, "Analytical expressions for the electromagnetic mode density in finite, one-dimensional,

photonic band-gap structures," *Phys. Rev. E.*, Vol. 53, 4107–4121, 1996.

44. Cheng, J.-Y and L.-W. Cheng, "Polarization-dependent filters based on chiral photonic structures with defects," *J. Opt. A: Pure and Applied Optics*, Vol. 7, 558–566, 2005.

45. Southwell, W. H., "Spectral response calculations of rugate filters using coupled-wave theory," *J. Opt. Soc. Am. A*, Vol. 5, 1558–1564, 1988.

46. Biot, M. A., "General theorems on the equivalence of group velocity and energy transport," *Phys. Rev.*, Vol. 105, No. 4, 1129–1137, 1957.

47. Gerasik, V. and M. Stastna, "Complex group velocity and energy transport in absorbing media," *Phys. Rev. E.*, Vol. 81, 056602, 2010.